Structures of the icosahedral clusters in Ni–Nb–Zr–H glassy alloys determined by first-principles molecular dynamics calculation and XAFS measurements

ARTICLE *in* JOURNAL OF ALLOYS AND COMPOUNDS · MAY 2010

Impact Factor: 3 · DOI: 10.1016/j.jallcom.2010.02.188

5 AUTHORS, INCLUDING:

Mikio Fukuhara
Tohoku University
179 PUBLICATIONS **1,439** CITATIONS
SEE PROFILE

Hiroshi Oji
Japan Synchrotron Radiation Research Inst…
64 PUBLICATIONS **805** CITATIONS
SEE PROFILE

Akihisa Inoue
Josai International University
2,718 PUBLICATIONS **55,491** CITATIONS
SEE PROFILE

Shuichi Emura
Osaka University
268 PUBLICATIONS **2,873** CITATIONS
SEE PROFILE

Journal of Alloys and Compounds 497 (2010) 182–187

Contents lists available at ScienceDirect

Journal of Alloys and Compounds

journal homepage: www.elsevier.com/locate/jallcom

Structures of the icosahedral clusters in Ni–Nb–Zr–H glassy alloys determined by first-principles molecular dynamics calculation and XAFS measurements

M. Fukuhara[a,*], N. Fujima[b], H. Oji[c,d], A. Inoue[a], S. Emura[e]

[a] Institute for Materials Research, Tohoku University, 2-1-1 Katahira, Aoba, Sendai 980-8577, Japan
[b] Faculty of Engineering, Shizuoka University, Hamamatsu 432-8561, Japan
[c] Industrial Application Division, Japan Synchrotron Radiation Research Institute, 1-1-1 Kouto, Sayo-cho, Sayo-gun, Hyogo 678-5198, Japan
[d] SPring-8 Service Co., Ltd., 2-23-1 Kouto, Kamigori-cho, Ako-gun, Hyogo 678-1205, Japan
[e] Institute of Scientific and Industrial Research, Osaka University, 8-1 Mihoga-oka, Ibaraki, Osaka 567-0047, Japan

ARTICLE INFO

Article history:
Received 2 February 2010
Received in revised form 18 February 2010
Accepted 27 February 2010
Available online 6 March 2010

Keywords:
Amorphous alloys
Structure of clusters
XAFS
Ab initio calculations
Fine structure

ABSTRACT

To elucidate the hydrogen localization sites in the atomic clusters of Ni–Nb–Zr–H glassy alloys exhibiting room-temperature Coulomb oscillation, we investigated the effect of hydrogen on the electronic state of the elements forming the glassy alloys, as well as the coordinating position of the hydrogen atoms, by X-ray absorption fine structure (XAFS) analysis, referencing theoretical simulation results. The XANES (X-ray absorption near edge structure) part of the XAFS spectra for each (Ni, Zr and Nb) K-edge of $(Ni_{0.36}Nb_{0.24}Zr_{0.40})_{89}H_{11}$ shows clear multiple scattering effects caused by charged hydrogen atoms. The distorted $Ni_5Zr_5Nb_3$ cluster with the maximum size of 0.55 nm is characterized by five Ni atoms constituting half a pentahedron and an opposite pentahedral Zr–Nb assembly. For the hydrogen localization sites, the first-principles calculations show that there are two Zr–Zr–Nb–Nb, four Zr–Zr–Zr–Nb, two Zr–Zr–Nb–Ni and two Zr–Zr–Zr–Ni tetrahedrons, in the order of stability.

1. Introduction

Following the theoretical pioneering work of Ben-Jacob and Gefen [1] and the subsequent discovery of the Coulomb blockade effect caused by quantum-dot tunneling at low temperatures [2,3], a number of studies have been reported to achieve room-temperature oscillation [4–9]. Recently, Fukuhara et al. have observed the Coulomb oscillation in $((Ni_{0.6}Nb_{0.4})_{0.7}Zr_{0.3})_{100-y}H_y$ ($5.2 \le y \le 15.2$) [10–12], $((Ni_{0.6}Nb_{0.4})_{1-x}Zr_x)_{100-y}D_y$ ($x = 0.30$, 0.35, 0.40 and 0.45, $9.1 \le y \le 14.8$) [13] and Ti–Ni–Cu–H [14] glassy alloys. Following these two-terminal Coulomb dot oscillations, we observed room-temperature switching, Coulomb blockade and memory effects in a millimeter-sized three-terminal glassy alloy field-effect transistor (GAFET) [15]. Based on our AC impedance analyses, we regard the glassy alloy as a DC/AC converting device with a high number of femto F capacitors comprised of regular prisms separated from the clusters by an average distance of 0.23 nm [16]. However, in order to convince many researchers in the field of electric and electronic engineering of these results, we must provide an accurate visualization of the atomic configuration of the nanometer-sized clusters which compose the millimeter-sized glassy alloys.

To analyze the atomic configuration of the clusters in Ni–Nb–Zr–H alloys, we investigated the atomic configuration around the Ni, Nb and Zr atoms by X-ray absorption fine structure (XAFS) spectroscopy [17]. By analyzing the EXAFS (extended X-ray absorption fine structure) part in the XAFS spectra measured at the Ni, Nb and Zr K-edges in the glassy alloys, we found that hydrogen charging in the glassy alloys does not alter the local structures around the three atoms in the Zr30at% alloy, but induces an elongation of the Zr–Zr, Zr–Nb and Nb–Ni distances in the Zr40at% alloy. The difference in structural response to hydrogen charging between the Zr30 and Zr40at.% alloys probably derives from the difference in the sites where the hydrogen atoms are located. In previous report we considered that hydrogen atoms in the Zr30at.% alloy plunge into a space somewhere outside the clusters, based on the consideration that there is no change in the bond length, while the elongation of the Zr–Zr/Zr–Nb and Nb–Ni distances in the $(Ni_{36}Nb_{24}Zr_{40})_{0.89}H_{0.11}$ (Zr40-H11) alloy is associated with the occupation by hydrogen of the tetrahedral sites surrounded by Zr and Nb or Zr, Nb, and Ni atoms in the clusters[18]. In fact, the Zr-40at.% alloy showed room-temperature Coulomb oscillation when it was hydrogenated, while the Zr30at.% alloy did not. Thus, the origin of the difference in the electronic properties of these alloys lies in the structural difference between them. Based on the results of

* Corresponding author. Tel.: +81 22 215 2610; fax: +81 22 215 2381.
E-mail address: fukuhara@imr.tohoku.ac.jp (M. Fukuhara).

0925-8388/$ – see front matter © 2010 Elsevier B.V. All rights reserved.
doi:10.1016/j.jallcom.2010.02.188

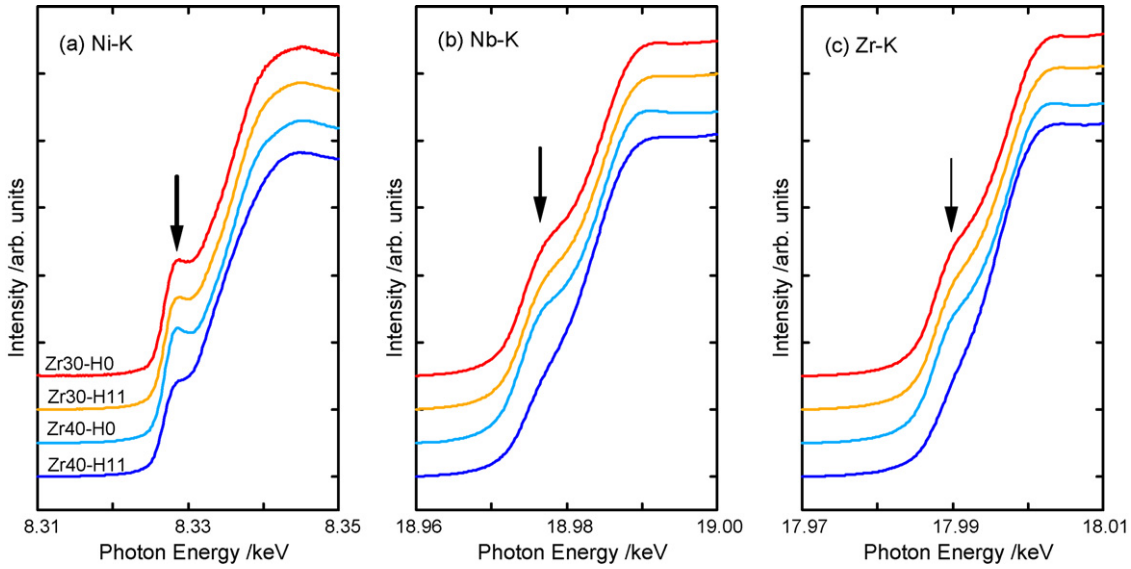

Fig. 1. Close-ups of pre-edge peaks in XANES spectra of the glassy alloys at the (a) Ni, (b) Nb, and (c) Zr K-edges.

the EXAFS analysis, we propose two possible structure models for the Ni–Nb–Zr glassy alloy with 40at.%Zr [17]. On the other hand, the X-ray Absorption Near Edge Structure (XANES) spectrum includes structural information which is complementary to the information afforded by EXAFS. Especially, the spectra of the pre-edge region reflect the electronic structure of the relevant ion and its surroundings, as is well known. We found that the hydrogen atoms occupy highly symmetric sites in Zr40-H11, to prevent the *d–p* mixing, and that hydrogen atoms principally surround the Zr and Nb atoms [19].

In the present paper, we discuss in detail a possible cluster model for the glassy alloys. First, we examine the XAFS data again, focusing on the XANES spectra, in order to extract further structural information, especially related to the possible position of the hydrogen atoms inside the cluster. Also, the results of the cluster simulation of the Zr40at.% alloy by first-principles calculations are presented. This gives a more probable hydrogen position than the model proposed based on the analysis of the EXAFS and XANES spectra. The stable hydrogen sites are discussed based on the results of the XAFS and theoretical simulation.

2. Experimental and computational methods

The rotating wheel method under an argon atmosphere was used for the preparation of glassy alloy $\{(Ni_{0.6}Nb_{0.4})_{100-x}Zr_x\}_{100-y}$-$H_y$ (x = 30,35,40,45 and 50, $5.2 \leqq y \leqq 22$) ribbons with a width of ~1 mm and a thickness of ~30 μm from argon arc-melted ingots. Hydrogen charging was carried out electrolytically in 0.5 M H_2SO_4 and 1.4 g/L thiourea (H_2NCSNH_2) at room temperature and at a current density of 30 A/m^2, using a Pt counter electrode. The details of the procedure have been described in previous papers [10–12].

The XAFS spectra were measured at the bending magnet beamline, BL14B2, of SPring-8. The incident X-rays were monochromatized by a silicon double crystal monochromator. The net planes used were (3 1 1) for the Nb and Zr K-edges and (1 1 1) for the Ni K-edge. To obtain the appropriate X-ray absorption intensity, the two sheets of ribbon (~42 μm) were stacked in the Nb K-edge and Zr K-edge measurements in order to obtain the necessary thickness, while one sheet of ribbon (~21 μm) had the optimum thickness for the Ni K-edge measurements. The samples were cooled down to ~20 K to reduce the thermal disorder.

The optimized atomic configurations of the icosahedral clusters that consisted of Ni, Nb, Zr and H atoms were determined by VASP, a plane-wave-based first-principles molecular dynamics calculation package [20]. We employed the ultrasoft pseudopotential for the core orbitals [21] (1s–3p for Ni and 1s–4p for Zr and Nb) under the generalized gradient approximation (PW91 [22]). The cut-off energy for the plane wave basis was 241.622 eV (NORMAL precision in VASP). The isolated cluster system was realized in a supercell with the Γ-point approximation. A length of more than 10 Å was adopted for the cell dimension. A quasi-Newtonian algorithm was used to relax the ions until the change in the total energy reached below 10^{-3} eV between two ionic steps. The results of the simulation were compared with those of the XAFS analysis to construct the optimum cluster model.

3. Results

3.1. Analysis of the XANES spectra

The electronic states around the outmost shell of the absorbing atom should be reflected in the pre-edge energy region, where transitions from a 1*s* orbital to an *nd*, an $(n+1)d$ and an $(n+1)p$ state can be observed in transition metals. The former two transitions are essentially forbidden, while the last one is allowed for the electric dipole moment. Therefore, the absorption intensities of the former two transitions are weak, but very sensitive to the alignment symmetry of the surroundings. A few pre-edge peaks were often observed in the XAFS spectra of transition metal compounds. Weak but explicit pre-peaks were sometimes found, and were assigned to the transition to the *nd* states. Fig. 1 shows the absorption spectra around the K-edge of Ni, Nb and Zr, respectively, for the Ni–Nb–Zr–H glassy alloys. The rising of each absorption edge is accompanied by a shoulder, except in the case of the Zr40–H11 alloy. The energy position of the shoulder is in the range of 1–5 eV below the edge determined as the energy position having half the intensity of the edge jump. Therefore, it is reasonable to assign the shoulder peaks to the parity forbidden transition to the 3*d* orbital (Ni) and the 4*d* orbital (Nb and Zr). The transition moment to the orbitals generally does not reach zero, due to the crystal (ligand) field with odd parity or the lattice vibration (phonon) of odd parity modes in solids. As can be seen in Fig. 1, the intensity of the shoulder for the Zr30at.% alloy remains unchanged in hydrogenation at all three absorption edges. However, that for the Zr40at.% alloy is substantially weakened by hydrogenation at the Nb and Zr K-edges, although less affected at the Ni K-edge.

Turning our attention to the post-edge energy region in the XANES spectrum, a difference between Zr30% and Zr40% was similar to that in the pre-edge region on the hydrogenation of the alloys. The difference in the post-edge region for the XANES spectrum would include structural information on the cluster backbone complementary to the information given by the EXAFS spectra. Moreover, the scattering caused by light elements such as H, He, and Li diminished at a low wavenumber, because the back-scattering amplitudes rapidly decreased with the wavenumber of the photo-

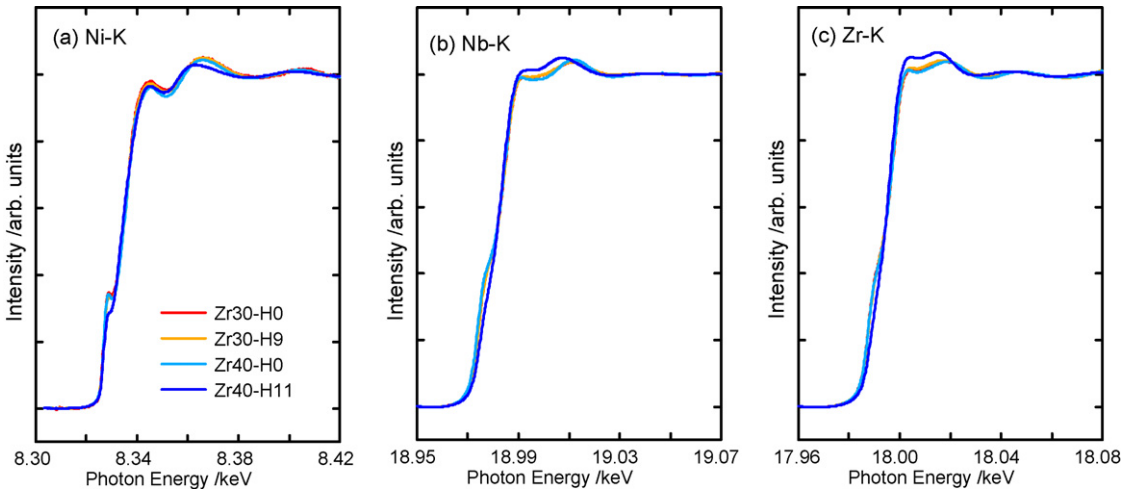

Fig. 2. XANES spectra of the glassy alloys at (a) Ni, (b) Nb and (c) Zr K-edges including pre- and post-edge-regions.

Table 1
Comparison between the calculated and the experimental coordination numbers for the Zr–Ni, Zr–Zr or Zr–Nb and Nb–Ni bondings in four kinds of simulated clusters.

Cluster type		Centred element	Coordination numbers		
Cluster type	Total binding energy (eV)		Zr–Ni	Zr–Zr or Zr–Nb	Nb–Ni
1. Ih553i	−79.8289	Zr	2.40	4.80	1.00
2. Ih553z	−79.157	Zr	2.60	4.60	1.67
3. Ih553b	−78.8349	Zr	1.40	4.60	2.00
4. Ih553e	−77.2815	Zr	2.00	5.20	3.33
XAFS result			2.6	5.1	0.90

electrons. Since the kinetic energy of the photo-electrons in the XANES region was much lower than that in the EXAFS region, the spectra were directly and considerably affected even by these light elements. For these reasons, the XANES part of the XAFS spectra was more sensitive to the coordination of the H atoms than the EXAFS part. Thus, we were also able to inspect the effects of hydrogenation on the structure from the post-edge XANES spectra.

As shown in Fig. 2, the post-edge spectrum of the Zr40at.% alloy for the Ni K-edge was less affected by the hydrogenation. On the other hand, those for the Nb and Zr K-edges were rather strongly modified by the hydrogenation. In the case of the Zr30at.% alloy, almost no change was observed upon hydrogen doping. Here, it should be noted that the modification of the spectrum by the charged hydrogen showed a similar tendency for both the Nb and Zr K-post-edges. This finding implies that the multi-scattering paths of the hydrogen atoms surrounding these metal atoms were analogical: that is, the hydrogen atoms coordinated around these metal atoms in a similar electronic configuration in both cases. The results shown in Fig. 2 are consistent with the structural configurations yielded by the XANES analysis, shown in Fig. 1. The results of the XANES analysis described above strongly suggest the following several points: (i) In Zr30at.% glassy alloys, the hydrogen atoms do not localize inside, but outside the clusters. (ii) The hydrogen atoms rarely localize the position around Ni atoms. (iii) The hydrogen atoms occupy the suitable sites in the clusters in the Zr40at.% alloy, and localize around the Nb and Zr atoms but not around the Ni atoms. (iv) The sites occupied by the hydrogen atoms are positions which prevent *p–d* hybridization. This suggests that these possible positions have the high site symmetries. This deeper discussion again supports the model proposed by us in Ref. [17].

3.2. Simulation of the structure by first-principles calculations and the determination of the positions of the hydrogen atoms

To clarify the mechanism of the room-temperature Coulomb oscillation observed in $(Ni_{0.36}Nb_{0.24}Zr_{0.40})_{90}H_{10}$ glassy alloy, we focus on the Zr40% sample with hydrogen in this section. Applying the coordination numbers obtained from the XAFS analysis results to the cluster model simulation by first-principles calculations, we reconstructed the atomic cluster model. It is well known that the

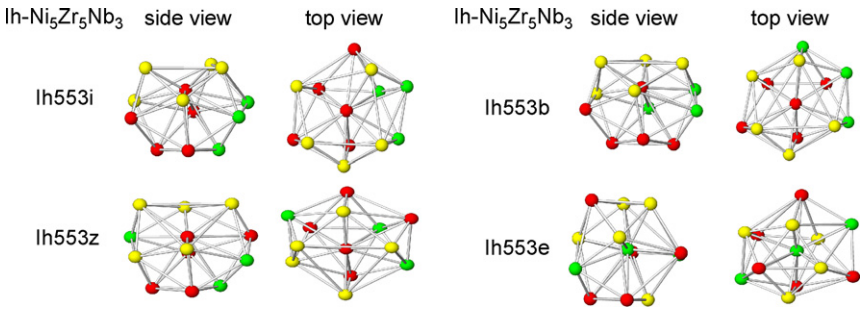

Fig. 3. Side and top views of the four stable kinds of simulated Zr5Ni5Nb3 clusters. The solid circles represent Zr atoms (red), Nb atoms (green), and Ni atoms (yellow). (For interpretation of the references to color in this figure legend, the reader is referred to the web version of the article.)

atomic clusters of metal/metal-typed glassy alloys are characterized by a Zr-centered icosahedral structure [23]. So, we focus on isolated icosahedral Zr-centered $Ni_5Nb_3Zr_5$ clusters, whose composition is close to that of the $Ni_{36}Nb_{24}Zr_{40}$ alloy [17], assuming that the energy of the hydrogen on the surface of the cluster is not significantly changed by the presence of neighboring clusters [18]. Real clusters are combined with small amounts of other Voronoi-like polyhedra: *i.e.*, they are not isolated [23]. The four possible structural models are presented in Table 1, along with the total binding energies, which are given for each structural model in the order of stability. The four kinds of models are shown in Fig. 3 with the side and top views.

The relationships between the coordination numbers of the Zr–Zr (or Zr–Nb) and Nb–Ni bondings, on the one hand, and the coordination numbers of the Zr–Ni bonding, on the other, are shown in Fig. 4. When applying the calculated coordination numbers for the four kinds of clusters to the experimental ones, the coordination numbers of Ih553z and Ih553i agree well with those determined by EXAFS analysis. Thus, the Ih553z and Ih553i clus-

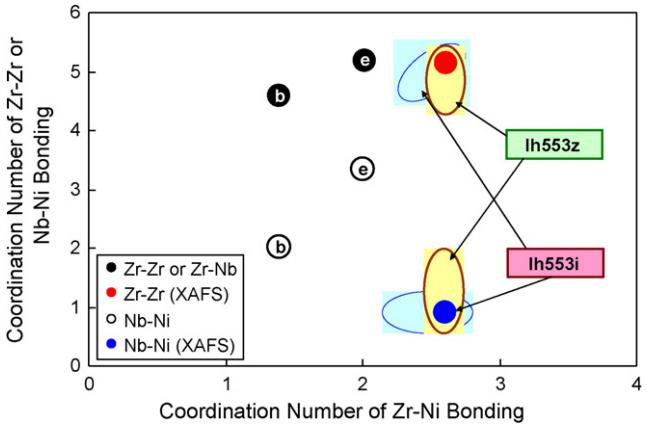

Fig. 4. Comparison between the calculated and the experimental coordination numbers for the Zr–Zr or Zr–Nb and Nb–Ni bondings in four stable kinds of simulated clusters.

facet H-distance (A)	side view	top view	facet H-distance (A)	side view	top view
Indices of hydrogen atoms	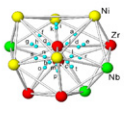	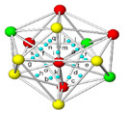			
(a) NiNiZr + 0.98	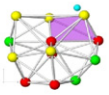	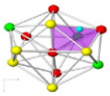	(k) NiNiNi + 0.85	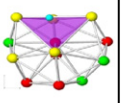	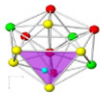
(b) NiNiZr + 0.96	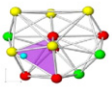	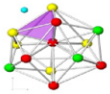	(l) ZrZrNb - 0.66	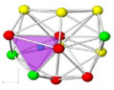	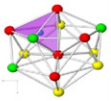
(c) NiNiNb* (NiZrNb) + 0.64	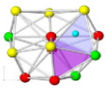	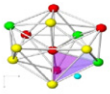	(m) ZrZrNb - 0.69	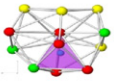	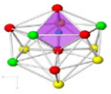
(d) NiNiNb + 0.54	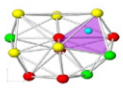	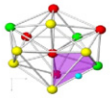	(n) ZrZrNb - 0.71	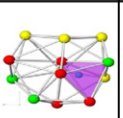	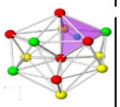
(e) NiNiNb* (NiZrNb) + 0.83	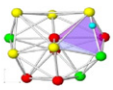	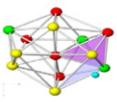	(o) NiZrZr - 0.32	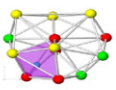	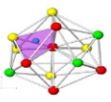
(f) NiNiNb + 1.04	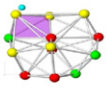	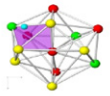	(p) ZrZrNb - 0.67	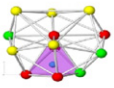	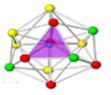
(g) NiNiNb + 0.87	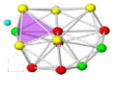	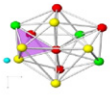	(q) NiZrNb - 0.56	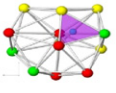	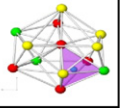

Fig. 5. The side and top views of 20 kinds of simulated $Zr_5Ni_5Nb_3$ clusters with H atom. The clusters are in the order of stability. The distance from the facet surface of the cage is also shown. The plus sign of the distance denotes running away from the center of the purple tetrahedral cage, while larger negative values mean stable localization of hydrogen in the one.

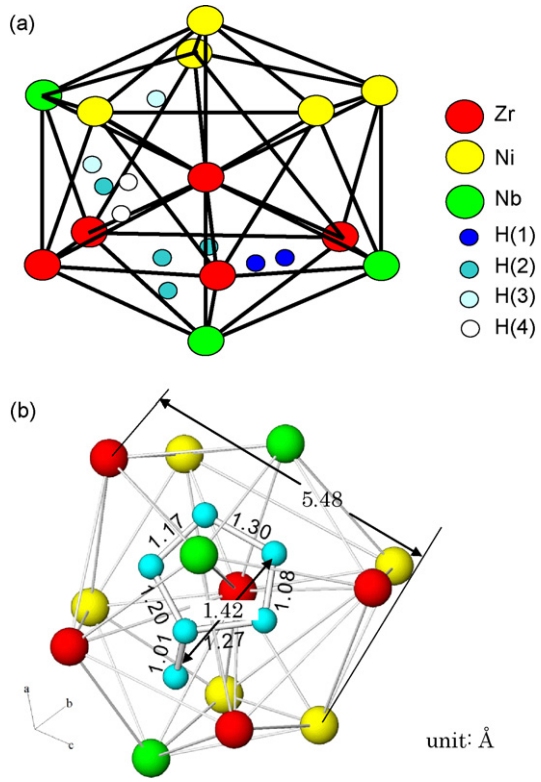

Fig. 6. (a) Hydrogen-occupied icosahedron cluster (Ih553z) model, and (b) the distances among two stable and four metastable H sites.

ter are candidates for the main intrinsic cluster. From the energetic point of view, the Ih553i cluster is the more feasible, as seen in the total energies listed in Table 1. However, as seen in Fig. 3, the shape of Ih553i and Ih553z is too distorted relative to the ideal icosahedron shape. In comparison with two models, the Ih553z cluster is slightly more stable than Ih553i one. Therefore we believe at this moment that the Ih533z cluster is the most probable cluster.

Next, we simulated the possible localization site of hydrogen in the hypothetical Ih553z icosahedron. A hydrogen atom was placed at the center of one of the 20 tetrahedron cages as its initial position (distance from the central Zr atom = 1.32 Å). Then, the position of the H atom was optimized relative to the fixed cages. When one hydrogen atom plunged into a tetrahedral site in the Ih553z icosahedron, the total energy of the Zr–Ni–Nb–H network changed depending on the combination of the three constituent elements of the for tetrahedron. The optimized positions of the H atom in the 20 possible kinds of $Ni_5Zr_5Nb_3$ (Ih553z) configurations are presented in Fig. 5, along with the distance from the facet surface of the cage. It should again be noted that the initial position of the H atom was set at the center of the purple tetrahedral cage. A plus sign on the distance denotes movement away from the tetrahedral cage, while larger negative values mean the stable localization of the hydrogen atom in the cage. Actually, the hydrogen atom in Fig. 5(c) and (e) moves away from the tetrahedrons composed of two or three Ni elements ((a)–(i) and (k) in Fig. 5), and settle inside the tetrahedron with zero or one Ni atom ((j)). As a result, the order of stability of the hydrogen site in the tetrahedrons is as follows: two Zr–Zr–Nb–Nb ((r) and (t)), four Zr–Zr–Zr–Nb ((l)–(n) and (p)), two Zr–Zr–Nb–Ni ((q) and (s)) and two Zr–Zr–Zr–Ni ((j) and (o)) tetrahedrons. Since Ni has an anti-affinity for hydrogen, the sites of the last two Zr–Zr–Ni–Ni tetrahedra are metastable, while the sites of the two Zr–Ni–Ni–Ni and Zr–Nb–Ni–Ni tetrahedral afford negligibly small stability. These results for the optimum hydrogen site are summarized in Fig. 6, which also ten hydrogen atoms. For clarity, the model cluster is illustrated in the regular icosahedron shape in the figure, although it is distorted in reality. The distances of inter hydrogen atoms among the two stable and four metastable H sites are presented in Fig. 6(b).

4. Discussion

In the previous paper [18], we have affirmed that $(Ni_{0.36}Nb_{0.24}Zr_{0.40})_{100-y}H_y$ $(0 \le y \le 20)$ glassy alloys show semiconductivity, superior electric transport at room temperature, superconductivity (onset temperature = 10 K) and electron avalanche behaviours, and electric current-induced voltage (Coulomb) oscillation, as the hydrogen content increases. These findings suggest that the effect of hydrogen localization outside and inside the clusters plays important roles in various electron transport phenomena. From the calculated adiabatic potential energy of the hydrogen atom for the distorted icosahedral $Zr_5Ni_5Nb_3$ cluster with hydrogen, it was concluded that the potential energy of hydrogen adsorbed by the outer surface of the cluster was lower than that of the bonding state between Zr (or Nb) and the H atoms settled in the cluster [18,24]. In other words, the outer adsorbed hydrogen of the cluster is in a stable state, while the inner bonding hydrogen in the tetrahedron is in a metastable state. Indeed, the hydrogen atom localized to a site between the clusters in alloys with a hydrogen content of approximately 5 at%, and inside the clusters in alloys with a hydrogen content between 7 at% and 12.5 at% [18]. The above calculation results are in good agreement with the XANES results about affinity elements for hydrogen.

It is known that the icosahedral clusters with a size of ~1 nm exist in metal/metal-typed Zr-based glassy alloys with a Zr-centered cluster [23]. Since our model, Ih553z, is a Zr-centered icosahedral $Zr_5Ni_5Nb_3$ cluster with a maximum size of 0.55 nm, the atomic configuration agrees with the results of the XAFS analysis, shown in Fig. 3. The glassy alloy used in the present study consists of antinomic elements (*i.e.*, Zr and Nb show affinity and Ni anti-affinity for hydrogen). Indeed, the enthalpies of the dissolved hydrogen atoms for Zr, Nb and Ni are −63, −34 and +16 kJ/mol H, respectively [25]. Thus, we must take the antinomy into consideration when we examine the structure of icosahedral clusters with hydrogen as well as conventional hydrogenated crystals. As can be seen from the sign of the distance from the facet surface of the cage in Fig. 5, the most stable localization site for hydrogen is the tetrahedral site formed by two Zr and two Nb atoms, while the tetrahedron consisting of three Zr atoms and one Nb atoms is of secondary stability. The hydrogen is less stable if it is at a tetrahedral site which includes at least one Ni atom. Thus, the distorted $Ni_5Zr_5Nb_3$ cluster of interest is characterized by five Ni atoms which form half a pentahedron and an opposite pentahedral Zr–Nb assembly, because the theoretical simulations indicate that the gathering of Ni atoms in the icosahedra lowers the total energy. The nanometer-sized strangely shaped icosahedral clusters and their atomic configurations seem to be the source of functional properties such as the Coulomb oscillation [10–15], superconductivity and ballistic transport [18] behaviours.

5. Conclusion

The XANES spectra of the $Ni_{42}Nb_{28}Zr_{30}$ and $Ni_{36}Nb_{24}Zr_{40}$ glassy alloys were analyzed, including the pre-edge region, and the effects of hydrogenation of the glassy alloys and the coordinating position of the hydrogen atoms were discussed. The XANES spectra at each (Ni, Zr and Nb) K-edge of $(Ni_{0.36}Nb_{0.24}Zr_{0.40})_{89}H_{11}$ showed a clear multi-scattering effect caused by the charging of the hydrogen atoms. The edge shoulder vanished or weakened, suggesting the conversion of the electronic state of the metal ions owing to the

hydrogenation. The selective hydrogen localization into the icosahedral clusters for the Ni–Nb–Zr glassy alloy was investigated by comparing the calculated and the experimental coordination numbers. As a result, we propose the Ih553z cluster as the most suitable cluster model, which has a Zr-centered icosahedral structure with the maximum size of 0.548 nm. The most stable hydrogen site is formed by two tetrahedra consisting of two Zr and two Nb atoms. The next stable site is formed by two tetrahedra consisting of three Zr atoms and one Nb atom.

Acknowledgements

This work was supported by a Grant-In-Aid for Science Research in the priority Area 'Research and Development Project on Advanced Metallic Glasses, Inorganic Materials and Joining Technology' from the Ministry of Education, Science, Sports and Culture, Japan, and by the JSPS Asian CORE Program. The synchrotron radiation experiments were performed with the approval of the Japan Synchrotron Radiation Research Institute (JASRI) (Proposal No. 2007B1820).

References

[1] E. Ben-Jacob, Y. Gefen, Phys. Lett. 108A (1985) 289.
[2] M.A. Kastner, P.F. Kwasnick, J.C. Licini, D.J. Bishop, Phys. Rev. B 36 (1987) 8015.
[3] T.A. Fulton, G.J. Dolan, Phys. Rev. Lett. 59 (1987) 109.
[4] K. Yano, T. Ishi, T. Hashimoto, T. Kobayashi, F. Murai, IEEE Trans. Electron. Dev. 41 (1994) 1628.
[5] H. Ishikuro, T. Fujii, T. Saraya, G. Hashiguchi, T. Hiramoto, T. Ikoma, Appl. Phys. Lett. 68 (1996) 3585.
[6] L. Guo, E. Leobandung, S.Y. Chou, Science 275 (1997) 649.
[7] S.J. Tans, A.R.M. Verschueren, C. Decker, Nature 393 (1998) 49.
[8] R. Martel, T. Schmidt, H.R. Shea, T. Hertel, Ph. Avouris, Appl. Phys. Lett. 73 (1998) 2447.
[9] H.W.Ch. Postma, T. Teepen, Z. Yao, M. Grifoni, C. Dekker, Science 293 (2001) 76.
[10] M. Fukuhara, A. Kawashima, S. Yamaura, A. Inoue, Appl. Phys. Lett. 90 (2007) 203111.
[11] M. Fukuhara, S. Yamaura, A. Inoue, J. Phys.: Conf. Ser. 144 (2009) 012086.
[12] M. Fukuhara, A. Inoue, J. Appl. Phys. 105 (2009) 063715.
[13] M. Fukuhara, A. Inoue, Europhys. Lett. 83 (2008) 36002.
[14] M. Fukuhara, S. Yamamura, A. Inoue, Phys. Stat. Solid. B 246 (2009) 153.
[15] M. Fukuhara, M. Seto, A. Inoue, Appl. Phys. Lett. (submitted for publication).
[16] M. Fukuhara, M. Seto, A. Inoue, Appl. Phys. Lett. 96 (2010) 043103.
[17] H. Oji, K. Handa, J. Ide, T. Honma, S. Yamaura, A. Inoue, N. Umesaki, S. Emura, M. Fukuhara, J. Appl. Phys. 105 (2009) 113527.
[18] H. Oji, K. Handa, J. Ide, T. Honma, N. Umesaki, S. Yamaura, M. Fukuhara, A. Inoue, S. Emura, J. Phys. Conf. Ser. 190 (2009) 012075.
[19] G. Kresse, J. Furthenüller, Comput. Mater. Sci. 6 (1996) 15.
[20] D. Vanderbilt, Phys. Rev. B41 (1996) 7892.
[21] J.P. Perdew, J.A. Chevary, S.H. Vosko, K.A. Jackson, M.R. Pederson, D.J. Singh, C. Fiolhais, Phys. Rev. B46 (1991) 6671.
[22] T. Fukunaga, K. Itoh, T. Otomo, K. Mori, M. Sugiyama, H. Kato, M. Hasegawa, A. Hirata, Y. Hirotsu, A.C. Hannon, Mater. Trans. 48 (2007) 1698.
[23] M. Fukuhara, H. Yoshida, K. Koyama, A. Inoue, Y. Miura, J. Appl. Phys. 107 (2010) 033703.
[24] M. Fukuhara, H. Yoshida, A. Inoue, N. Fujima, Intermetallics, in press.
[25] R.B. McLellan, W.A. Oates, Acta Metall. 21 (1973) 181.